GEOPHYSICAL RESEARCH LETTERS, VOL. 35, L15301, doi:10.1029/2008GL034723, 2008

Imaging compaction band propagation in Diemelstadt sandstone using acoustic emission locations

Edward Townend,[1] Ben D. Thompson,[2] Philip M. Benson,[1,2] Philip G. Meredith,[1] Patrick Baud,[3] and R. Paul Young[2]

Received 18 May 2008; revised 28 June 2008; accepted 3 July 2008; published 2 August 2008.

[1] We report results from a conventional triaxial test performed on a specimen of Diemelstadt sandstone under an effective confining pressure of 110 MPa; a value sufficient to induce compaction bands. The maximum principal stress was applied normal to the visible bedding so that compaction bands propagated parallel to bedding. The spatio-temporal distribution of acoustic emission events greater than 40 dB in amplitude, and associated with the propagation of the first compaction band, were located in 3D, to within ±2 mm, using a Hyperion Giga-RAM recorder. Event magnitudes were used to calculate the seismic b-value at intervals during band growth. Results show that compaction bands nucleate at the specimen edge and propagate across the sample at approximately 0.08 mm s^{-1}. The seismic b-value does not vary significantly during deformation, suggesting that compaction band growth is characterized by small scale cracking that does not change significantly in scale.
Citation: Townend, E., B. D. Thompson, P. M. Benson, P. G. Meredith, P. Baud, and R. P. Young (2008), Imaging compaction band propagation in Diemelstadt sandstone using acoustic emission locations, *Geophys. Res. Lett.*, *35*, L15301, doi:10.1029/2008GL034723.

1. Introduction

[2] Compaction bands have been reported in the field [*Mollema and Antonellini*, 1996; *Sternlof et al.*, 2004], in laboratory studies [*Olsson*, 1999; *Wong et al.*, 2001; *Fortin et al.*, 2006] and in numerical simulations [*Sternlof et al.*, 2005; *Katsman and Aharonov*, 2006; *Wang et al.*, 2008], and are defined as localised deformation features that orient normal or sub-normal to σ_1. Within compaction bands, intensive comminution and interpenetration of grains leads to porosity and grain size reduction [*Wong et al.*, 2001]. Results from both field [*Sternlof et al.*, 2004] and laboratory [*Vajdova et al.*, 2004] studies suggest that permeability may be decreased by several orders of magnitude across compaction bands. Since high-porosity sandstones, considered as analogues for reservoir rocks, have been shown experimentally [*DiGiovanni et al.*, 2000] to be susceptible to compaction band development, their existence in nature has significant implications for crustal fluid circulation.

[3] Acoustic emissions (AE), resulting from brittle cracking, have long been used to monitor the accumulation of crack damage that leads to failure in studies of rock deformation [e.g., *Mogi*, 1968; *Scholz*, 1968; *Sammonds et al.*, 1992]. More recently, AE locations have been used to identify the distribution of such damage [e.g., *Lockner et al.*, 1991; *Olsson and Holcomb*, 2000; *Benson et al.*, 2007]. In particular, *Fortin et al.* [2006] have used AE locations to map the development of progressive sequences of compaction bands as a function of strain during the deformation of porous sandstone.

[4] In contrast to the study of *Fortin et al.* [2006], we have used a fast, multi-channel, full-waveform AE monitoring system to locate and track the spatial and temporal evolution of a single, discrete, compaction band across the full diameter of a core sample of Diemelstadt sandstone. We also characterise the scale of cracking during the band development from the magnitude-frequency distribution (seismic b-value) of located AE events.

2. Experimental Material, Equipment, and Methods

[5] Cylindrical samples of Diemelstadt sandstone, 100 mm long and 40 mm in diameter, were prepared using a diamond coring drill, with the ends ground flat and parallel to within 0.01 mm. The material comprises 65% quartz, 15% feldspar, 10% lithics, and 10% micas and accessory oxides. It has a porosity of approximately 24% and an average grain diameter of 100 μm. The sample material used was visibly anisotropic, specifically selected because this study forms part of a larger study on the influence of anisotropy on compactive deformation. The anisotropy arises primarily from the anisotropic distribution of pore space, and has been characterized as horizontal transverse isotropy (HTI) from measurements of the magnetic susceptibility anisotropy of ferro-fluid saturated void space [*Townend et al.*, 2006]. It is worthy of note, therefore that our sample material is significantly different in microstructure from the more homogeneous Diemelstadt sandstones used by *Baud et al.* [2004] and *Louis et al.* [2006] in their studies on compaction bands. The sample used in this study was cored normal to the bedding plane; parallel to the minimum anisotropy axis. However, as a result of small-scale cross bedding, the axis of minimum anisotropy can be up to 20° from the core axis in individual samples.

[6] Conventional, drained, triaxial experiments were performed using the stiff, servo-controlled triaxial deformation apparatus at University College London described by *Benson et al.* [2007]. Samples were jacketed in nitrile rubber and deformed under drained conditions to 3.5% axial strain, at a constant axial strain rate of 10^{-5} s^{-1}, and under a confining pressure of 120 MPa. A constant

[1]Rock and Ice Physics Laboratory, Department of Earth Sciences, University College London, London, UK.
[2]Lassonde Institute, University of Toronto, Toronto, Ontario, Canada.
[3]Institut de Physique du Globe, Strasbourg, France.

0094-8276/08/2008GL034723

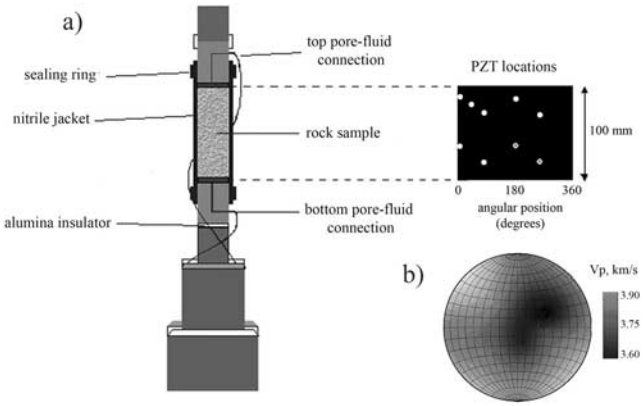

Figure 1. (a) Sample assembly and unwrapped view of the nitrile sample jacket showing positions of the PZT crystals. Crossed circles denote source crystals, and open circles denote receiving crystals used during P-wave velocity surveys. (b) Stereographic projection of the velocity structure of the Diemelstadt sandstone sample at an effective hydrostatic confining pressure of 110 MPa.

pore pressure of 10 MPa was maintained via two servo-controlled pore pressure intensifiers, yielding an effective pressure of 110 MPa. Previous studies had indicated that these were appropriate conditions for inducing compaction bands in this material [*Townend et al.*, 2006].

[7] AE hits above a threshold of 40 dB were recorded continuously throughout the experiment by means of nine piezo-electric transducers (PZT crystals), of 1 MHz central frequency, mounted on stainless steel inserts embedded in the rubber sample jacket. The sample assembly and transducer locations are shown in Figure 1. The same transducers were used to make sequential wave velocity measurements to characterize the changing velocity structure of the sample during deformation. All outputs were received, digitized and recorded on a Hyperion Giga-RAM recorder at 10 MHz [*Thompson et al.*, 2005, 2006]. The criterion for the location of AE events was that hits should be recorded on a minimum of six out of the nine transducers. This ensured a location accuracy of better than ±2 mm [*Benson et al.*, 2007]. Seismic b-values were computed, from the magnitudes of located events only, using the maximum likelihood method of *Aki* [1965]. In order to ensure statistical rigor, each b-value was calculated from a rolling window of 200 event magnitudes.

3. Experimental Results

[8] Compressional wave velocities (Vp) were measured under a hydrostatic effective confining pressure of 110 MPa, before the application of any differential stress, along 14 ray-paths created by using 2 of the PZT transducers as transmitters and 7 as receivers. The 3D velocity structure obtained from the inversion of the travel times along all 14 ray-paths is presented as a stereographic projection in Figure 1. The Vp anisotropy at 110 MPa hydrostatic pressure is approximately 10%, with the minimum Vp sub-normal to the visible bedding and the maximum and intermediate Vp sub-parallel to bedding. The inverted velocity data were then used in a TI simplex algorithm for the 3D location of AE events.

[9] Figure 2 shows the mechanical data from an experiment performed at an effective pressure of 110 MPa. The stress-strain curve deviates from linearity at a differential stress of approximately 125 MPa and an axial strain of about 1.4%. This deviation is accompanied by an associated increase in AE activity that marks the point where the sample starts to accommodate strain through the brittle micro-cracking associated with grain crushing. We therefore interpret this point as C*, the critical stress for the onset of shear-enhanced compaction [*Wong et al.*, 1997]. Following C*, the stress-strain curve rolls over and then plateaus with a small degree of strain hardening. The AE rate continues to increase during the roll-over phase, attaining a maximum around 2.2% axial strain. AE rate then decreases to become steady at around 3% axial strain. The total number of AE hits recorded during the experiment was approximately 900,000, of which 11,000 source events were located using the location criteria noted earlier.

[10] Figure 3 shows the locations of AE events during the four back-to-back 125 second time windows labeled 1 to 4 on Figure 2. These time windows cover the peak in AE activity over the strain range 1.8% to 2.3%; the period during which the first compaction band nucleated and propagated. The located data are presented as two orthogonal elevations and a plan view. The elevations show all the events located during the growth period (a total of 1800) but, for clarity, the plan view shows only the events located within the band indicated by the two arrows on the upper part of Figure 3.

[11] We first note two zones of relatively diffuse AE activity close to the sample ends. There is an end constraint on the sample caused by the mismatch between the elastic modulus of the rock and that of the steel loading rams. The sample ends therefore effectively see a larger compressive stress than the main volume of the sample. During compactive deformation this leads to enhanced cracking and AE activity at the sample ends. By contrast, during dilatant

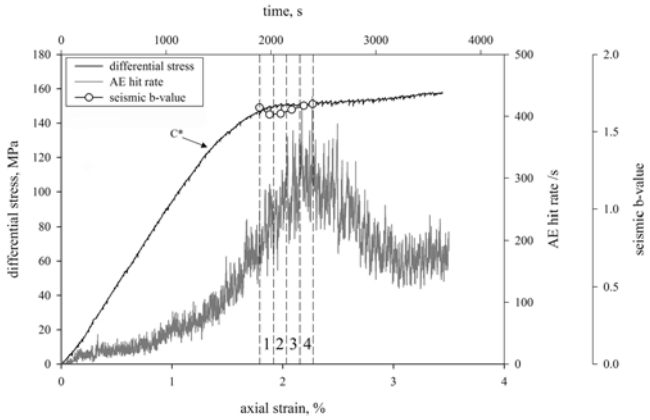

Figure 2. Stress-strain curve and AE hit rate for the Diemelstadt sandstone sample deformed under an effective confining pressure of 110 MPa and a strain rate of 10^{-5} s^{-1}. C* marks the critical stress for the onset of shear enhanced compaction, and the bands marked 1 to 4 indicate four sequential time windows during nucleation and propagation of the first compaction band. Seismic b-values, calculated from AE events located during compaction band growth, are also plotted.

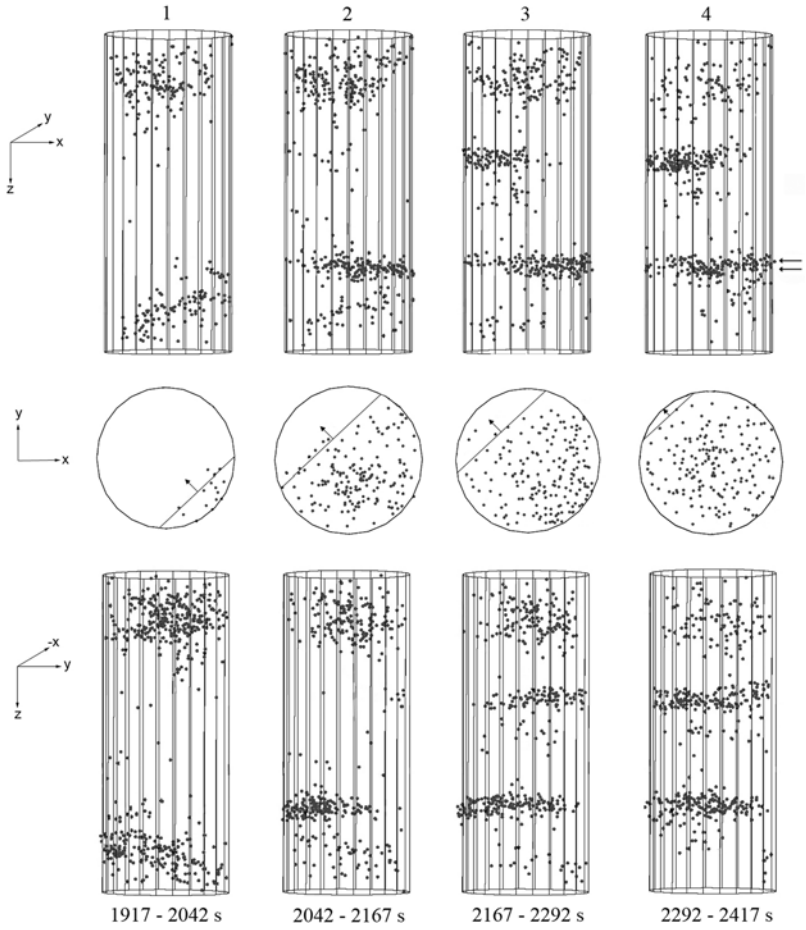

Figure 3. AE locations associated with the propagation of the first compaction band; shown as two orthogonal elevations and a plan view. The numbers at the top correspond to the time windows shown in Figure 2, with the absolute timings shown at the bottom. The two arrows on the upper right diagram indicate the extent of data used for the plan view, and the Cartesian axes indicate the relative orientations of the projections.

deformation this leads to reduced cracking and relative seismic quiescence at the sample ends [e.g., *Benson et al.*, 2007].

[12] Around 1.8% axial strain, we observe a small cluster of AE events at the edge of the sample at about one-third height (window 1 in Figure 3). This marks the nucleation of the first discrete compaction band, which then propagates across the sample (windows 2 to 4) in a plane essentially normal to the direction of σ_1. The plan views of the propagating AE cluster in Figure 3 show that it has a relatively straight leading edge; shown as lines that encompass 95% of the located events. The leading edge traverses approximately 30 mm across the sample in 375 seconds, which allows us to estimate an average propagation speed of about 0.08 mm s^{-1}. We also observe that a second compaction band starts to propagate at about two-thirds of the sample height before the first band has completely traversed the sample (starting during time window 2). The orthogonal elevations in Figure 3 show that this second band propagates across the sample in a plane parallel to the first band, but in a direction approximately normal to it.

[13] The magnitudes of all AE events were determined by centroid moment tensor analysis after locations and onset times had been determined. Seismic b-values were then calculated using a rolling window of 200 events. This gives a standard error of less than 10%. The calculated b-values are presented in Figure 2, superimposed on the stress-strain curve. The b-value remains essentially constant (within the standard error) at around 1.6 during the whole of the compaction band propagation. Finally, Figure 4 (left) shows an image of the recovered sample after 3.5% axial strain, taken in the Y-Z plane (same direction as the lower images in Figure 3). Figure 4 (right) shows all located AE events from time-windows 1–4 superimposed on the image of the recovered sample.

4. Discussion and Conclusions

[14] Consistent with field observations [*Mollema and Antonellini*, 1996; *Sternlof et al.*, 2004] and laboratory studies [*Olsson*, 1999; *DiGiovanni et al.*, 2000; *Baud et al.*, 2004], we report experimental observations of the propagation of compaction bands oriented normal to the direction of σ_1. Our results demonstrate that the nucleation of the first compaction band occurs at a stress level just beyond the onset of shear-enhanced compaction, and therefore in the transitional regime between brittle faulting and cataclastic flow [*Wong et al.*, 2001]. Spatio-temporal locations of AE events show that compactive deformation,

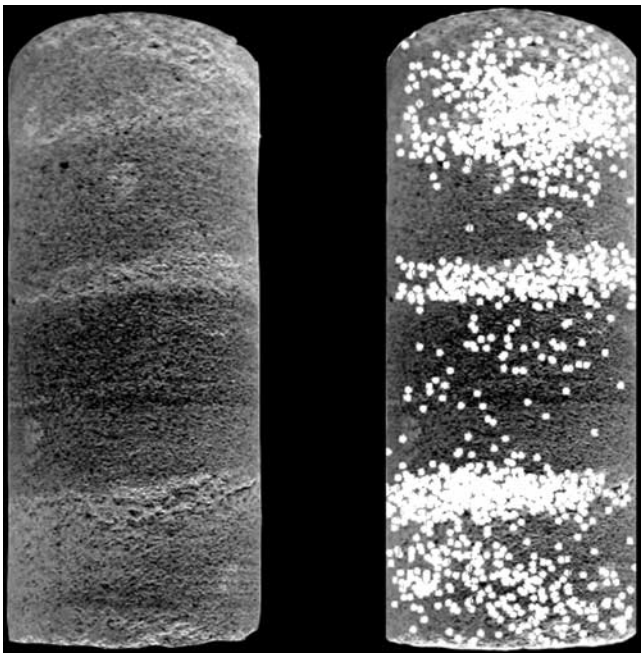

Figure 4. (left) Image of the exterior surface of the sample recovered after 3.5% axial strain, taken in the Y-Z plane, showing discrete compaction bands and diffuse damage at the sample ends. (right) Located AE events from time windows 1–4 superimposed on the image to demonstrate the spatial correlation.

characterized by the growth of discrete compaction bands, is a relatively slow process, with the propagation speed being less than 0.1 mm s^{-1}. This is in marked contrast to dilatant deformation, characterized by shear localization, which occurs several orders of magnitude faster [e.g., *Benson et al.*, 2007]. The ratio of the speed of compaction band propagation to the loading piston velocity is approximately 80:1. This is in good agreement with the ratio of approximately 100:1 reported by *Vajdova and Wong* [2003], as inferred from the duration of AE surges associated with compaction band growth.

[15] Figure 4 shows that the located AE events track the evolution of damage in our sample extremely well; both the diffuse damage that occurs at the sample ends on initial compression, and the discrete compaction bands that propagate at higher differential stress. Compaction band growth originates at the sample boundary before propagating across the sample with a relatively straight leading edge. Unlike for shear fault propagation [*Benson et al.*, 2007] we do not observe any zone of AE quiescence in the wake of the propagating compaction band. Rather, AE activity continues in the regions previously traversed by the band. We also observe that, although compaction bands appear to be spatially discrete and localized features, they appear not to be temporally discrete. We note above that a second compaction band begins to propagate before the first band has fully traversed the sample. The second band is located 35 mm above the first band, outside the zone of the sample affected by the end constraint. The second band also nucleates at the sample boundary, and propagates in a plane parallel to the first band, but in a quasi-orthogonal direction. Both bands are relatively planar and normal to the σ_1 direction, in marked contrast to the more tortuous bands described by *Louis et al.* [2006] and *Fortin et al.* [2006]. We interpret this difference as being due to the fact that our bands propagated sub-parallel to bedding in a highly anisotropic rock, whereas the bands described by *Louis et al.* [2006] and *Fortin et al.* [2006] were propagating in more homogeneous, and presumably more isotropic, material.

[16] The seismic b-value characterizes the magnitude-frequency distribution of AE events. If the magnitude of an individual AE event is related to the increment of crack growth producing it, then any change in the b-value during deformation is an indicator of a change in the scale of cracking [*Main et al.*, 1989; *Meredith et al.*, 1990]. Here, we observe a relatively high and constant b-value of around 1.6 during compaction band nucleation and growth, suggesting that such compactive deformation is characterized by small scale cracking that does not change in dimension during propagation. This is consistent with a grain-scale cracking and pore collapse deformation mechanism, and with the observation of an essentially constant, slow compaction band propagation speed. These observations are in marked contrast to the b-value minimum commonly observed during dilatant deformation, associated with dynamic failure and localization on a shear fault [*Meredith et al.*, 1990].

[17] **Acknowledgments.** This work was partially supported by a Natural Environment Research Council (NERC) studentship award to ET, a Marie-Curie International Fellowship within the 6th European Community Framework program to PMB (contract MOIF-CT-2005-020167), a Royal Society/CNRS scientific exchange award to PGM and PB (contract 17338), and a Natural Sciences and Engineering Research Council (NSERC) discovery grant to RPY. We benefited from fruitful discussions with Teng-fong Wong, Sheryl Tembe, and Laurent Louis.

References

Aki, K. (1965), Maximum likelihood estimate of the parameter b in the formula log N = a − bm and its confidence limits, *Bull. Earthquake Res. Inst. Univ. Tokoyo*, *43*, 237–239.

Baud, P., E. Klein, and T.-F. Wong (2004), Compaction localization in porous sandstones: Spatial evolution of damage and acoustic emission activity, *J. Struct. Geol.*, *26*, 603–624.

Benson, P. M., B. D. Thompson, P. G. Meredith, S. Vinciguerra, and R. P. Young (2007), Imaging slow failure in triaxially deformed Etna basalt using 3D acoustic-emission location and X-ray computed tomography, *Geophys. Res. Lett.*, *34*, L03303, doi:10.1029/2006GL028721.

DiGiovanni, A. A., J. T. Fredrich, D. J. Holcomb, and W. A. Olsson (2000), Micromechanics of compaction in an analogue reservoir sandstone, in *Proceedings of the Fourth North American Rock Mechanics Symposium*, pp. 1153–1160, Rotterdam, Brookfield, Vt.

Fortin, J., S. Stanchits, G. Dresen, and Y. Gueguen (2006), Acoustic emission and velocities associated with the formation of compaction bands in sandstone, *J. Geophys. Res.*, *111*, B10203, doi:10.1029/2005JB003854.

Katsman, R., and E. Aharonov (2006), A study of compaction bands originating from cracks, notches, and compacted defects, *J. Struct. Geol.*, *28*, 508–518.

Lockner, D., J. D. Byerlee, V. Kuksenko, A. Ponomarev, and A. Sidorin (1991), Quasistatic fault growth and shear fracture energy in granite, *Nature*, *350*, 39–42.

Louis, L., T.-F. Wong, P. Baud, and S. Tembe (2006), Imaging strain localization by x-ray computed tomography: Discrete compaction bands in Diemelstadt sandstone, *J. Struct. Geol.*, *28*, 762–775.

Main, I. G., P. G. Meredith, and C. Jones (1989), A reinterpretation of the precursory seismic b-value anomaly from fracture mechanics, *Geophys. J. Int.*, *107*, 353–362.

Meredith, P. G., I. G. Main, and C. Jones (1990), Temporal variations in seismicity during quasi-static and dynamic rock failure, *Tectonophysics*, *175*, 249–268.

Mogi, K. (1968), Source locations of elastic shocks in the fracturing process in rocks, *Bull. Earthquake Res. Inst. Univ. Tokyo*, *46*, 1103–1125.

Mollema, P. N., and M. A. Antonellini (1996), Compaction bands: A structural analog for anti-mode I cracks in aeolian sandstone, *Tectonophysics*, *267*, 209–228.

Olsson, W. A. (1999), Theoretical and experimental investigation of compaction bands in porous rock, *J. Geophys. Res.*, *104*, 7219–7228.

Olsson, W. A., and D. J. Holcomb (2000), Compaction localization in porous rock, *Geophys. Res. Lett.*, *27*, 3537–3540.

Sammonds, P. R., P. G. Meredith, and I. G. Main (1992), Role of pore fluids in the generation of seismic precursors to shear fracture, *Nature*, *359*, 228–230.

Scholz, C. H. (1968), Experimental study of the fracturing process in brittle rock, *J. Geophys. Res.*, *73*, 1447–1453.

Sternlof, K., J. Chapin, D. D. Pollard, and L. J. Durlofsky (2004), Effective permeability in sandstones containing deformation band arrays, *AAPG Bull.*, *88*, 1315–1329.

Sternlof, K. R., J. W. Rudnicki, and D. D. Pollard (2005), Anticrack inclusion model for compaction, bands in sandstone, *J. Geophys. Res.*, *110*, B11403, doi:10.1029/2005JB003764.

Thompson, B. D., R. P. Young, and D. A. Lockner (2005), Observations of premonitory acoustic emission and slip nucleation during a stick slip experiment in smooth faulted Westerly granite, *Geophys. Res. Lett.*, *32*, L10304, doi:10.1029/2005GL022750.

Thompson, B. D., R. P. Young, and D. A. Lockner (2006), Fracture in Westerly granite under AE feedback and constant strain rate loading: Nucleation, quasi-static propagation, and the transition to unstable fracture propagation, *Pure Appl. Geophys.*, *163*, 995–1019.

Townend, E., P. Baud, and P. G. Meredith (2006), The influence of anisotropy on the yield-cap and transport properties of Diemelstadt sandstone during a dilatant-compactant transition in deformation mode, *Eos Trans. AGU*, *87*(52), Fall Meet. Suppl., MR01-2087.

Vajdova, V., and T. Wong (2003), Incremental propagation of discrete compaction bands: Acoustic emission and microstructural observations on circumferentially notched samples of Bentheim, *Geophys. Res. Lett.*, *30*(14), 11775, doi:10.1029/2003GL017750.

Vajdova, V., P. Baud, and T.-F. Wong (2004), Permeability evolution during localized deformation in Bentheim sandstone, *J. Geophys. Res.*, *109*, B10406, doi:10.1029/2003JB002942.

Wang, B. S., Y. Chen, and T.-F. Wong (2008), A discrete element model for the development of compaction localization in granular rock, *J. Geophys. Res.*, *113*, B03202, doi:10.1029/2006JB004501.

Wong, T.-F., C. David, and W. Zhu (1997), The transition from brittle faulting to cataclastic flow in porous sandstone: Mechanical deformation, *J. Geophys. Res.*, *102*, 3009–3025.

Wong, T.-F., P. Baud, and E. Klein (2001), Localized failure modes in a compactant porous rock, *Geophys. Res. Lett.*, *28*, 2521–2524.

P. Baud, Institut de Physique du Globe, 5 rue Descartes, F-67084 Strasbourg, France.

P. M. Benson, P. G. Meredith, and E. Townend, Rock and Ice Physics Laboratory, Department of Earth Sciences, University College London, Gower Street, London WC1E 6BT, UK. (etownend@ikonscience.com)

B. D. Thompson and R. P. Young, Lassonde Institute, University of Toronto, 170 College Street, Room 108, Toronto, ON M5S 3E3, Canada.